Cavitation erosion performance of steel, ceramics, carbide and Victrex PEEK materials

Dr Spencer Court [1]*, Dr Ilaria Corni [2], and Dr Nicola Symonds [3]

ABSTRACT

Cavitation erosion has to be taken into consideration during material selection in many industrial sectors, e.g. offshore, marine and oil and gas, where the components operates under severe working conditions.

The cavitation erosion equipment, located at the University of Southampton (UoS), uses a vibratory apparatus to compare, rank and characterise the cavitation erosion performance of materials. This paper highlights some of the results obtained from industrial research (consultancy) work employing a Hielscher UIP1000hd 20 kHz ultrasonic transducer. The transducer is attached to a titanium horn to induce the formation and collapse of cavities in the liquid creating erosion (material loss) of the specimen under test.

The results from erosion cavitation testing (in accordance with ASTM G32) of two commercially available steels are presented and shown to have less resistance to cavitation when compared to PEEK, ceramics and carbide materials. These materials are presented along with Nickel 200 which was used to normalise the results. A plot of cumulative erosion vs exposure time was determined by periodic interruption of the test.

Keywords

Cavitation, erosion, vibratory apparatus, profilometry. PEEK, carbides, ceramic ASTM-G32,

[1],[2,3] nC[2] Consulting, Faculty of Engineering and the Environment, University of Southampton, Southampton, SO17 1BJ), * Author for correspondence s.w.court@soton.ac.uk

Introduction to the Paper

Cavitation erosion has to be taken into consideration during material selection in many industrial sectors, such as offshore, marine and oil and gas, where the components operates under severe working conditions. Cavitation erosion is a process where cavities or bubbles, that contain vapour or a mixture of vapour and gas, form in a liquid and then subsequently collapse on the surface of a solid material producing small diameter micro-jets impinging on to the surface at a speed of up to 200 m s^{-1}[1]. This process creates destructive shockwaves leading to erosion, pitting and surface wear. During cavitation-erosion, the rate of erosion of the tested material is not constant with time but goes through several stages [2]: incubation stage, acceleration stage, maximum rate stage and deceleration stage.

The study of cavitation erosion using vibratory apparatus is based on the ASTM G32 "Test Method for Cavitation Erosion Using Vibratory Apparatus" [2]. This methodology has been used extensively as a research tool for assessing the cavitation erosion resistance of various materials including metals and alloys. For instance Tallion et al. [3] have applied cavitation erosion to stainless steels with HVOF coatings and found using scanning electron microscopy (SEM) that the cavitation erosion mechanism in steels starts with crack formation in the grains and grain boundaries followed by material removal. Ahmed et al. [4] employed a SEM to observe the incubation period of vibratory cavitation erosion and concluded that the surface initially plastically deformed leading to wavey surface undulations and that the polishing lines had acted as initiation sites for pits. Hu et al. [5] compared the cavitated surfaces of Inconel 625 and Inconel 600 over time using SEM. This research indicated that hollows, from the impingement of collapsing bubbles, initiated along the grain boundaries which further degraded by plastic deformation and fracture. Zhen et al. [6] investigated Hastelloy C-276 nickel alloy

and compared it to 316 stainless steel. They reported the mechanism of cavitation erosion to be plastic deformation with initiation sites at the grain boundaries. Selective phase attack was also reported for the Hastelloy C-276 nickel based alloy. Basumatary et al. [7] who used various techniques to analyse the cavitation erosion of nickel aluminium bronze under cathodic protection also described selective phase attack. High speed cameras have also been employed to analyse the bubble formation emanating from the tip and compared this to abrasive particles [8]. It was found that the bubbles exploded asymmetrically with liquid filling the hollow to produce a liquid microjet.

The cavitation erosion behaviour of ceramics in various medias has been studied by Neibuhr et al. [9]. It was found that the ceramics exhibited an incubation stage of cavitation and had linear weight loss with the cavitation rate remaining constant over the duration of the test. The media did not affect the cavitation behaviour apart from when an acidic solution was employed, in this media the cavitation erosion resistance decreased. Lu et al. [10] have also reported the excellent cavitation resistance of Zirconia due to the fine grain size and few microstructural defects.

The cavitation erosion resistance of plastics has been studied by Hattori et al. [11] who examined materials such as epoxy resins and polypropylene. It was reported that the cavitation erosion was caused by fatigue fracture similar to that observed in metals. They also related the cavitation rate to the impact loads applied by bubble collapse. They showed that the impact load for plastics was lower than that for metals as plastics have very low acoustic impedances. Yamaguchi et al. [12] have also studied the cavitation erosion resistance of metals and plastics. The research showed that the maximum erosion rates of the metals occurred in the initial stages of cavitation and indicated that Victrex PEEK showed the highest erosion resistance of the plastics under test.

Studies have been also conducted to show the effect of the standoff distance in vibratory

equipment. Kikuchi et al. [13] measured the weight loss on aluminium, lead and stainless steel for distances between 0.1 mm and 6 mm. Each material was used as the vibratory tip or stationary specimen and their analysis showed that the weight loss was dependent on the material pair tested which either increased to a maximum or decreased with increasing separation. A review of the literature has shown the standoff distance to be between 0.5 mm and 2 mm with no recommendations being given in ASTM G32 [1-7]. The effect of temperature on the cavitation erosion resistance of materials is also well documented [14, 15] with studies showing that dependent on the type of material the erosion rate reaches a peak and then decreases. The ASTM G32 standard [2] suggests that the rate of cavitation is influenced by temperature peaking at about 50 ^{o}C. The standard also suggest that a temperature increase of 1 ^{o}C produces an increase in erosion rate of 1 or 2 %. Zhen et al. [16] studied the effect of temperature on the cavitation erosion of 304 stainless steel in water at elevated temperatures. They showed that up to 60 ^{o}C the eroded surface was uniform and that at 80 ^{o}C the surface gave the lowest cumulative mass loss with more localised and deep pits.

The aim of this paper is to study the effectiveness of the ASTM standard "Test Method for Cavitation Erosion Using Vibratory Apparatus" G32 as a tool to evaluate the resistance to cavitation erosion of different materials for industrial applications. Following the ASTM standard, nickel 200 has been used to verify the operation of the equipment at the University of Southampton (UoS) and subsequently to define the normalized erosion resistance of other tested materials.

The results from erosion cavitation testing (in accordance with ASTM G32) of two commercially available steels, two Victrex PEEK materials, carbides and ceramics will be presented. A plot of cumulative erosion vs exposure time was determined by periodic interruption of the test,

measuring mass loss and converting it to depth loss. The change in surface profile with erosion was recorded at intervals during the tests, using 2D contact and 3D optical profilometry. Scanning electron microscopy was also employed to examine the eroded material surfaces from above and in cross section.

EXPERIMENTAL PROCEDURE

The ultrasonic transducer employed for the tests was a Hielscher UIP1000hd 20 kHz (see Figure 1). The transducer was attached to a titanium horn to induce the formation and collapse of cavities in the liquid creating erosion (material loss) of the specimen under test. This instrument has a power rating of 1000W, 20 kHz with a peak-to-peak displacement amplitude of 50 ± 2 µm. Prior to each round of testing the sonotrode tip (tip diameter of 16 mm) was ground to a fine surface finish and the amplitude of the transducer was calibrated using a Keyence high speed, high accuracy CCD Laser Displacement sensor (LK-G32).

Before testing the sample was cleaned in isopropanol, dried using an air gun and weighed to 0.1 mg using a Mettler Toledo XP205 balance. The sample was fixed in a perspex bath and a gap of 0.5 mm (determined using a feeler gauge) was maintained between the sample and the tip surface. The position of the sample in relation to the tip was noted and 5 l of fresh distilled water was added to give a specimen depth of 15 mm to the top surface. During the test the temperature was kept constant at 25 ± 2 °C using a cooling plate so as not to disturb the cavitation process. The cavitation erosion test was interrupted every hour and the mass loss of the sample was measured and using the densities detailed in Table 1 the volume loss was calculated by dividing the cavitated area by the density to obtain a Mean Depth of Erosion (MDE).

TABLE 1: DENSITY OF THE MATERIAL TESTED

Material	Density / g cm^{-3}
Nickel 200 (UNS N02200)	8.91
High Tension Carbon Steel (HTCS)	7.85
Duplex Stainless Steel (DSS)	7.805
Victrex PEEK 1	1.3
Victrex PEEK 2	1.3
Tungsten Carbide (WC)	14.9
Silicon Carbide (SiC)	3.21
Zirconia (ZrO_2)	6.05

Commercially available nickel 200 (UNS N02200) (composition in weight%: 0.054% Co, 0.02% Cu, 0.1% Fe, 0.02% Mg, 0.25% Mn, 0.15% Si, <0.001% S and 99.38% Ni) supplied by Transvac Systems Ltd had the following dimensions: 25 mm x 25 ± 2 mm x 6 ± 0.5 mm.

The Victrex PEEK (PolyEtherEtherKetones) identified as Victrex PEEK 1 and Victrex PEEK 2 had dimensions of 25 mm x 25 ± 2 mm x 10 mm ± 0.5 mm and they were provided by Victrex.

The cavitation tests were run for 8 hours with periodic interruptions at hourly intervals. The 'as received' condition of all of the materials was used as the surface facing the cavitation horn.

The two steel materials used were: high tensile carbon steel (EN24T) and duplex stainless steel (UNS31803). The ceramics used were: silicon carbide and tungsten carbide and zirconia. All these materials were provided by Transvac Systems Ltd and had dimensions of 25 mm x 25 ± 2 mm x 5 mm ± 0.5 mm.

The profile of the nickel 200 was recorded over the duration of the test using a 2D contact profilometer (Form Talysurf 120L). The profile of the other tested materials was recorded after 8 hours of cavitation testing. Post cavitation exposure, the damaged surfaces were further

profiled with a 3D non-contact profilometry technique (Alicona Infinite Focus) which was used to measure a strip across the centre of each circular cavitation erosion patch. The nickel samples were also analysed using a JOEL (JSM6500F) SEM to determine the morphology of the surface at 30 min, 1 hour, 2 hours and 8 hours.

Sections of the two steel materials and of the ceramics were cut using a rotating diamond circular precision blade, the cross section samples were embedded in conductive polymer resin to create micros. These micros were then ground and polished to achieve high clarity. The grinding polishing stages were different for the two groups of materials (ferrous and ceramic). For the ferrous samples Struers Metalog Method E (MD-Piano + water, MD-Allegro + 9 μm, MD-Dur + 3 μm and MD-Chem + 0.04 μm) was followed. For the ceramics Method G (MD-Piano + water, MD Plan + 9 μm and MD-Chem + 0.04 μm) was followed. The samples and micros of the ceramic materials were then gold coated to provide electrical conductivity across the samples for examination in the scanning electron microscope (SEM). It was discovered that even with gold coating the zirconia micros could not be examined in the SEM, therefore high magnification optical microscopy was used.

RESULTS AND DISCUSSION

Erosion Cavitation Testing of Nickel 200 for Normalisation with the Standard

The cumulative erosion time curves for nickel 200 from the standard were compared to the results obtained using the ultrasonic vibratory system cavitation transducer (UIP1000hd) located at the UoS. The comparison plot of MDE per hour is provided in Figure 2 and a cumulative MDE plot is provided in Figure 3. The graphs indicate that the reproducibility of the tests carried out at the University are good although these samples exhibited a greater resistance to

cavitation than the nickel extrapolated from the ASTM G32.

From the graph of Cumulative MDE (Figure 3) the line of best fit was determined and this was extrapolated to zero to calculate the initiation period and the rate of erosion; the results of this analysis are reported in Table 2. From Table 2 it can be seen that the nickel tested at the UoS had a maximum rate of erosion of approximately 21.4 µm per hour and an incubation period of 75 minutes compared to data extrapolated from the ASTM G32 which had a maximum erosion rate of 29.9 µm per hour and an incubation time of 28 minutes.

TABLE 2: SUMMARY OF INCUBATION PERIODS AND RATE OF EROSION FOR NICKEL 200 CALCULATED FROM CUMULATIVE MEAN DEPTH OF EROSION GRAPHS

Material	Max Rate of cavitation [µm hr^{-1}]	Incubation Time [Min]
Nickel 200 run 1	19.782	75.8
Nickel 200 run 2	23.076	75.4
Nickel 200 run 3	21.408	64.5
Nickel ASTM G32	29.85	28.1

The UoS results showed a lower cavitation rate compared to the reference material in the standard. This could be due to differences in the material specification such as hardness. In fact, the hardness value reported in Table 1 of the ASTM G32 gave nominal ranges of 90 to 120 HB whereas the material certificate used in the UoS testing gave a hardness of 146 to 149 HB. This cavitation rate difference could be also due to the standoff distance between the sample and the horn employed during the test. The UoS testing was conducted with a standoff distance of 0.5 mm whereas the standard does not specify the distance used.

Figure 2 clearly shows that the maximum depth of erosion for the reference material in the standard was 35 μm per hour and this compares to an average of 20 μm for the Nickel 200 tested at the UoS. In order to normalise with the standard, therefore, the results have been multiplied by a factor of 35/20 and a summary plot of cumulative MDE with the normalisation applied is given in Figure 4. Since the results are all in agreement, it has been established that the data obtained at the UoS need to be multiplied by 35/20 in order to comply with the standard.

In order to confirm the depth of erosion over time, the profile of the cavitation damage was measured using contact profilometry before and during interruptions of the test. The results are not reported here but, as expected, they show the progression of the erosion over time. A comparison plot of MDE per hour recorded using the Talysurf against the mass loss data is provided in Figure 5 and a cumulative plot in Figure 6. These results indicate that the Talysurf measurements compare very closely to the mass loss method of determining depth of erosion and, therefore, demonstrate that the method employed was correct.

In order to assess the differences in incubation time (see Table 2) between the nickel tested at the UoS and that in the standard, the surfaces were examined employing an optical microscope after 30 min, 1 hour and 8 hours of testing. These images are reported in Figure 7. The surfaces show the progression of the cavities with time with a greater amount of cavitation damage formed at the edge.

Figure 8 shows SEM images of the same surfaces at a magnification of 30 x, 200 x and 750 x and backscattered images at 750 x magnification. The top row of images shows the surface profile prior to testing, where machining lines can clearly be seen. After 30 minutes the surface appears to be indented and this is clearly shown in the backscattered images with the machining line of the original nickel surface following the pattern of the indents. After 1 hour fractures on

the surface have begun to appear along the machining marks of the original nickel surface, which are still visible. After 8 hours of cavitation erosion cavities have increased and the original nickel surface can no longer be resolved. Overall, there appears to be a greater amount of cavities towards the edges of the cavitated area.

Images of cavitation for nickel 200 at several cumulative exposure times are presented in the standard and can be directly compared to the images presented in this study. After 30 minutes the surfaces are similar in appearance but after 8 hours the image shown in the standard seems to be more eroded, which would agree with the mass loss data showing a greater loss of mass for nickel 200 in the standard.

Erosion Cavitation Testing for Steels, Victrex PEEK, Carbides and Ceramics

The mass loss results for all the material tested are shown graphically in Figure 9 and show an increase in mass loss with exposure time. From the mean cumulative mass loss (Figure 10) the stages can be estimated. This is achieved by determining the line of best fit for the slope of the line to give the maximum erosion rate and extrapolating to zero to determine the incubation period.

The maximum MDE was for Victrex PEEK 1 and Victrex PEEK 2 and the materials with the lowest rates of erosion were tungsten carbide and zirconia. The mean incubation period and the max rate of erosion were calculated for each material and are reported in Table 3. Victrex PEEK 1 had a shorter incubation period and a higher maximum rate of erosion than the Victrex PEEK 2. The HTCS showed a shorter incubation period and a lower maximum rate of erosion compared with the duplex stainless steel. The tungsten carbide did not show an incubation period and had a very low erosion rate. The zirconia showed a high incubation time and a very

low rate of erosion, comparable to that of the tungsten carbide. The silicon carbide showed the highest max rate of erosion between the ceramic and carbide materials and the lowest incubation time after the tungsten carbide.

During the cavitation tests, the rate of erosion is not constant with time but goes through several stages. From the mean cumulative mass loss (Figure 10) the stages can be estimated. Overall, all of the materials exhibited an incubation stage, apart from the tungsten carbide and the zirconia. The acceleration stage and the maximum rate stages were also noted for the Victrex PEEK materials, the stainless steels and silicon carbide. The deceleration stage was not observed in any of the materials. No correlation has been found between the material hardness and the MDE values observed during the cavitation process.

TABLE 3: SUMMARY OF INCUBATION PERIODS AND MAXIMUM RATE OF EROSION FOR TESTED MATERIALS CALCULATED FROM NORMALISED CUMULATIVE MEAN DEPTH OF EROSION GRAPHS.

Material	Max Rate of erosion / $\mu m\ hr^{-1}$	Incubation Time / Mins
Tungsten Carbide	0.114	0.0
Zirconia	0.36	166.7
Silicon Carbide	2.028	36.5
High Tension Carbon Steel	8.994	200.1
Duplex Stainless Steel	10.65	253.5
Victrex PEEK 2	12.72	155.7
Victrex PEEK 1	28.704	125.4

The MDE calculated from the contact profilometry data after 8 hours of cavitation erosion testing was compared to the mass loss data prior to normalisation. For the Victrex PEEK

materials, the MDE was measured at 100 μm for Victrex PEEK 1 and at 60 μm for Victrex PEEK 2 using contact profilometry. The results from the non-contact profilometer (Alicona) gave a MDE of 110 μm for Victrex PEEK 1 and of 40 μm for Victrex PEEK 2. Similar trends were also noted for the steel, carbide and ceramic materials which showed the mass loss data having good agreement with the data obtained using the two profilometry techniques.

Analysis of the sample surfaces after Erosion Cavitation Testing

After cavitation testing circular areas of damage denoting the cavitation erosion were visible on each material. Zirconia and Tungsten Carbide samples showed an increase in the values of surface roughness through cavitation erosion. SEM and high magnification optical microscopy of the zirconia samples and the tungsten carbide samples from above and in cross-section revealed no evidence of subsurface cracking pre or post cavitation. Silicon carbide, High Tensile Carbon Steel and Duplex Stainless Steel samples showed wear scars that were deeper towards their centre; the damaged surfaces did not retain any original surface features such as machining marks and presented higher surface roughness. A cross section of the silicon carbide sample (Figure 11) showed subsurface cracking parallel to the surface at a depth of approximately 7 μm; this cracking would have released the next layer of material. SEM examination of the cross section of the Duplex Stainless Steel sample revealed that the material outside the cavitation zone was virtually un-affected leaving a vertical step in the material (Figure 12) and that the surface was removed in sections up to 50 μm deep (as shown by the depth of subsurface cracking in Figure 13). A cross section of the High Tensile Carbon Steel sample showed that the fracture surface appeared to contain many sharp stress-raisers and cracking within the top 20 μm (Figure 14). These structural findings are in agreement with the cavitation erosion results discussed in

the previous section.

CONCLUSIONS

Results from the cavitation erosion normalisation experiments showed that the nickel 200 tested at the UoS had a lower erosion rate and a higher incubation period when compared to the standard ASTM G32. When this was investigated further, SEM analysis showed that during the initial stages of cavitation the surface undergoes plastic deformation. This is characterised by a waviness appearance of the original machining lines, which was also reported by Hu et al. [5]. Following plastic deformation, the surface becomes fractured with initiation along the machining lines and with time this process continues to cover the whole of the surface.

In order to normalise our results with the standard, the data obtained at the UoS needed to be multiplied by a factor of 35 / 20. This adjustment does not affect the results generated when using the technique to rank the materials for resistance to cavitation. The data obtained using the two profilometry techniques were in good agreement with the mass loss data for all of the materials tested. This confirmed that the mass loss data gives an accurate indication of the depths of erosion produced.

The results discussed in this paper would suggest that the material tested could be ranked with decreasing resistance to cavitation erosion (more resistance materials first) in the following order:

1. Solid Tungsten Carbide
2. Solid Zirconia
3. Solid Silicon Carbide
4. High Tensile Carbon Steel

5. Duplex Stainless Steel

6. Victrex PEEK 2

7. Victrex PEEK 1

ACKNOWLEDGMENTS

nC^2 would like to thank Victrex plc and Transvac Systems Ltd for providing materials and funding to carry out this work.

REFERENCES

[1] Bournea N. K., Field J. E., "A high-speed photographic study of cavitation damage", *Journal of Applied Physics*, Vol. 78, 1995, 4423, https://doi.org/10.1063/1.359850.

[2] ASTM G32-10 "Standard Test Method for Cavitation Erosion Using Vibratory Apparatus".

[3] Taillon G., Pougoum F., Lavigne S., Ton-That L., Schulz R., Bousser E., Savoie S., Martinu L., Klemberg-Sapieha J. E., "Cavitation erosion mechanisms in stainless steels and in composite metal-ceramic HVOF coatings", *Wear*, Vol. 364-365, 2016, pp. 201–210, https://doi.org/10.1016/j.wear.2016.07.015

[4] Ahmed S. M., Hokkirigawa K., Ito Y., Oba R., "Scanning electron microscopy observation on the incubation period of vibratory cavitation erosion", *Wear*, Vol. 142, No. 2, 1991, pp. 303-314, https://doi.org/10.1016/0043-1648(91)90171-P

[5] Hu H. X., Zheng Y. G., Qin C. P., "Comparison of Inconel 625 and Inconel 600 in resistance to cavitation erosion and jet impingement erosion", *Nuclear Engineering and Design*, Vol. 240, No. 10, 2010, pp. 2721–2730, https://doi.org/10.1016/j.nucengdes.2010.07.021

[6] Li Z., Han J., Lu J., Chen J., "Cavitation erosion behavior of Hastelloy C-276 nickel-based alloy", *Journal of Alloys and Compounds*, Vol. 619, 2015, pp.754–759, https://doi.org/10.1016/j.jallcom.2014.08.248.

[7] Basumatary J., Wood R. J. K., "Different methods of measuring synergy between cavitation erosion and corrosion for nickel aluminium bronze in 3.5% NaCl solution", *Tribology International*, (in press) https://doi.org/10.1016/j.triboint.2017.08.006.

[8] Laguna-Camacho J. R., Lewis R., Vite-Torres M., Mendez-Mendez J. V., "A study of cavitation erosion on engineering materials", *Wear*, Vol. 301, No. 1-2, 2013, pp. 467–476,

https://doi.org/10.1016/j.wear.2012.11.026.

[9] Niebuhr D., “Cavitation erosion behavior of ceramics in aqueous solutions”, *Wear*, Vol. 263, No. 1-6, 2007, pp. 295–300, https://doi.org/10.1016/j.wear.2006.12.040.

[10] Lu J., Zum Gahrb K. H., Schneider J., “Microstructural effects on the resistance to cavitation erosion of ZrO_2 ceramics in water”, *Wear*, Vol. 265, No. 11-12, 2008, pp. 1680–1686, https://doi.org/10.1016/j.wear.2008.04.028.

[11] Hattori S., Itoh T., “Cavitation erosion resistance of plastics”, *Wear*, Vol. 271, No. 7-8, 2011, pp. 1103–1108, https://doi.org/10.1016/j.wear.2011.05.012.

[12] Yamaguchi A., Wang X., Kazama, T., "Evaluation of erosion-resisting properties of plastics and metals using cavitating jet apparatus," *SAE Technical Paper*, 2002-01-1386, 2002, https://doi.org/10.4271/2002-01-1386.

[13] Kikuchi K., Hammitt F. G., “Effect of separation distance on cavitation erosion of vibratory and stationary specimens in a vibratory facility”, *Wear*, Vol. 102, No.3, 1985, pp. 211–225, https://doi.org/10.1016/0043-1648(85)90219-4.

[14] Iwai Y., Okada T., Hammitt F.G., “Effect of temperature on the cavitation erosion of cast iron”, *Wear*, Vol. 85, No. 2, 1983, pp. 181-191, https://doi.org/10.1016/0043-1648(83)90062-5.

[15] Hattori S., Goto Y., Fukuyama T., “Influence of temperature on erosion by a cavitating liquid jet”, *Wear*, Vol. 260, No. 11-12, 2006, pp. 1217–1223, https://doi.org/10.1016/j.wear.2005.08.001.

[16] Li Z., Han J., Lu J., Zhou J., Chen J., “Vibratory cavitation erosion behavior of AISI304 stainless steel in water at elevated temperatures”, *Wear*, Vol. 321, 2014, pp. 33–37, https://doi.org/10.1016/j.wear.2014.09.012.

Figures

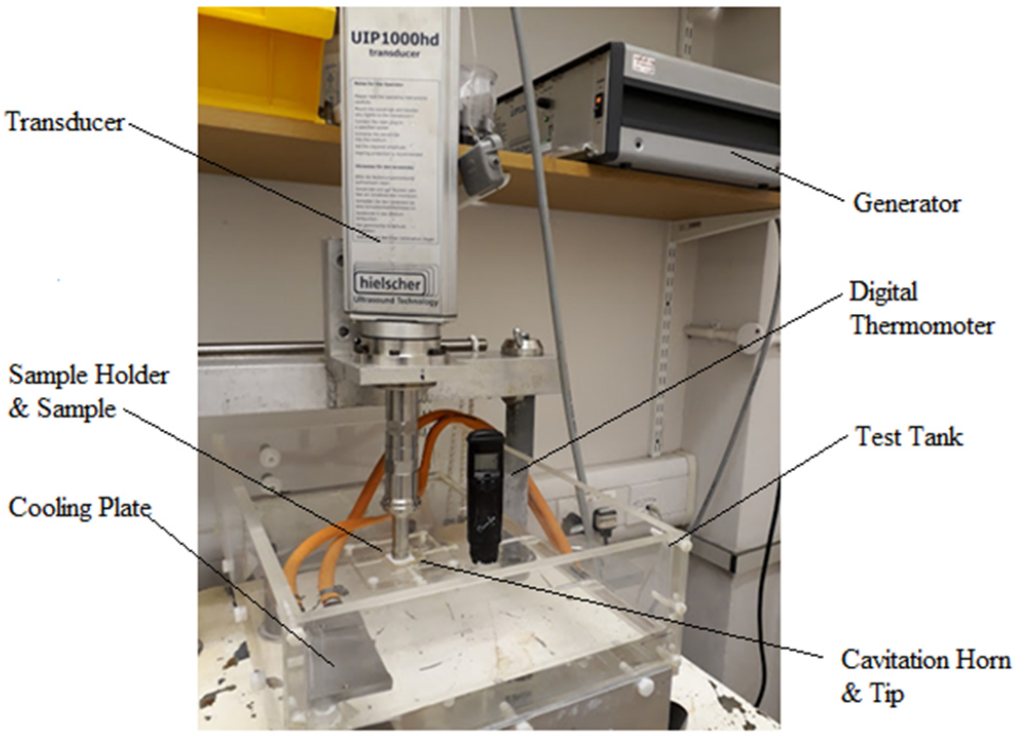

FIG. 1 CAVITATION EROSION TEST RIG.

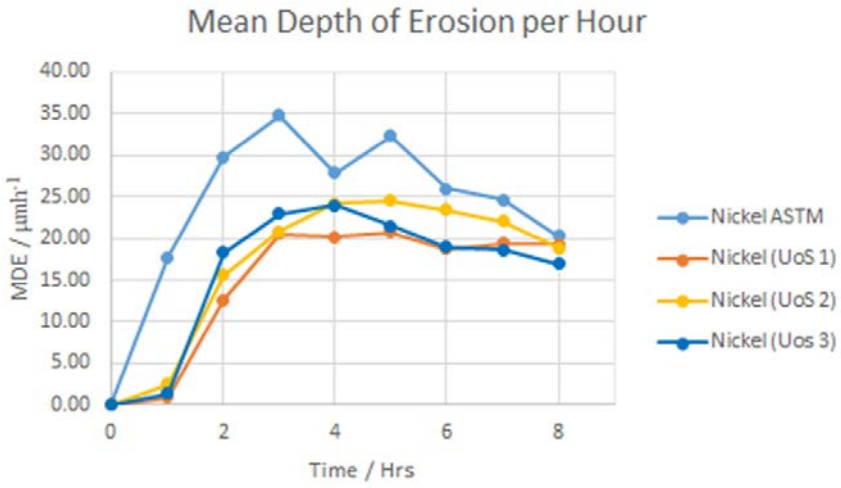

FIG. 2 GRAPH TO SHOW THE MEAN DEPTH OF EROSION PER HOUR FOR NICKEL 200 AS MEASURED IN ASTM G32 AND AT THE UOS.

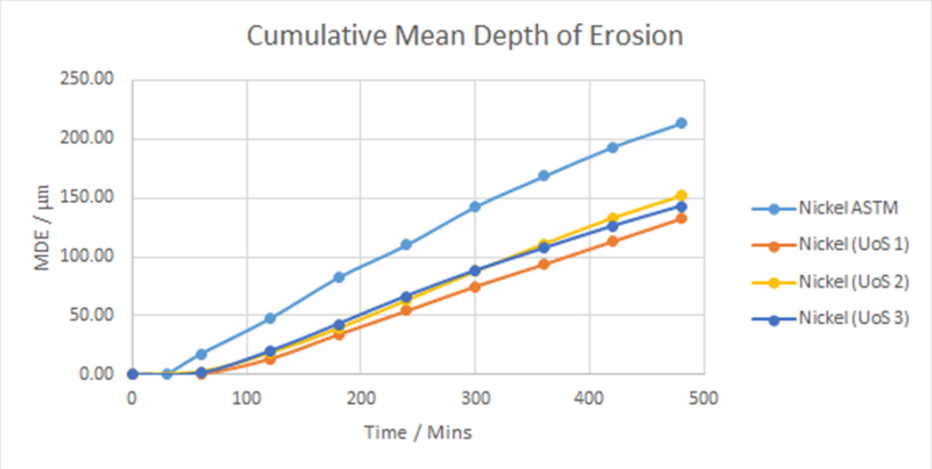

FIG.3 GRAPH TO SHOW THE CUMULATIVE MEAN DEPTH OF EROSION FOR NICKEL 200 AS MEASURED IN ASTM G32 AND AT THE UOS.

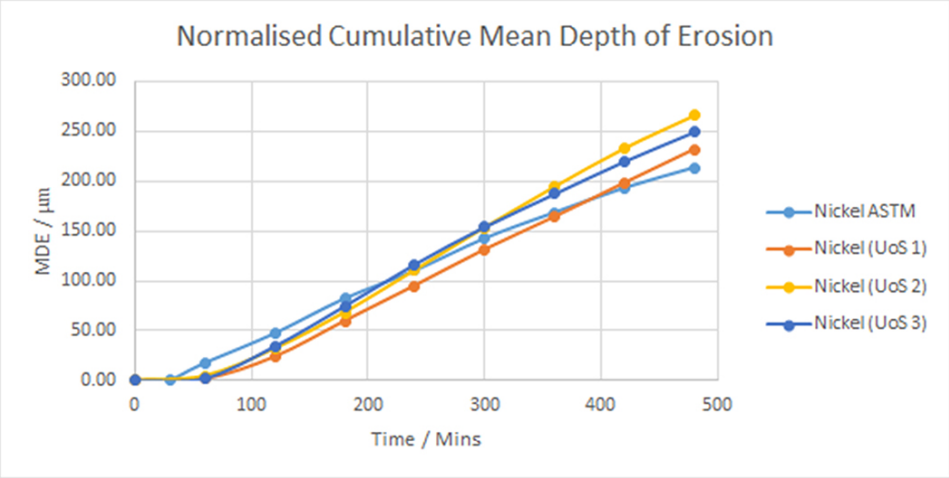

FIG. 4 GRAPH TO SHOW THE NORMALISED CUMULATIVE MEAN DEPTH OF EROSION FOR NICKEL 200 AS MEASURED IN ASTM G32 AND AT THE UOS.

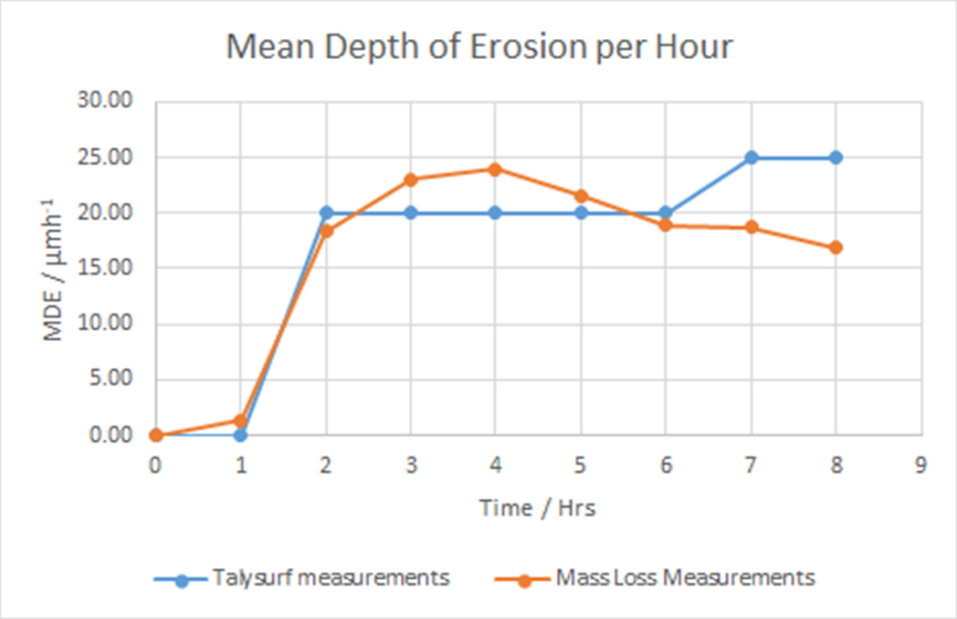

FIG. 5 GRAPH TO SHOW THE MEAN DEPTH OF EROSION PER HOUR FOR NICKEL 200 AS APPROXIMATED FROM TALYSURF AND MASS LOSS MEASUREMENTS.

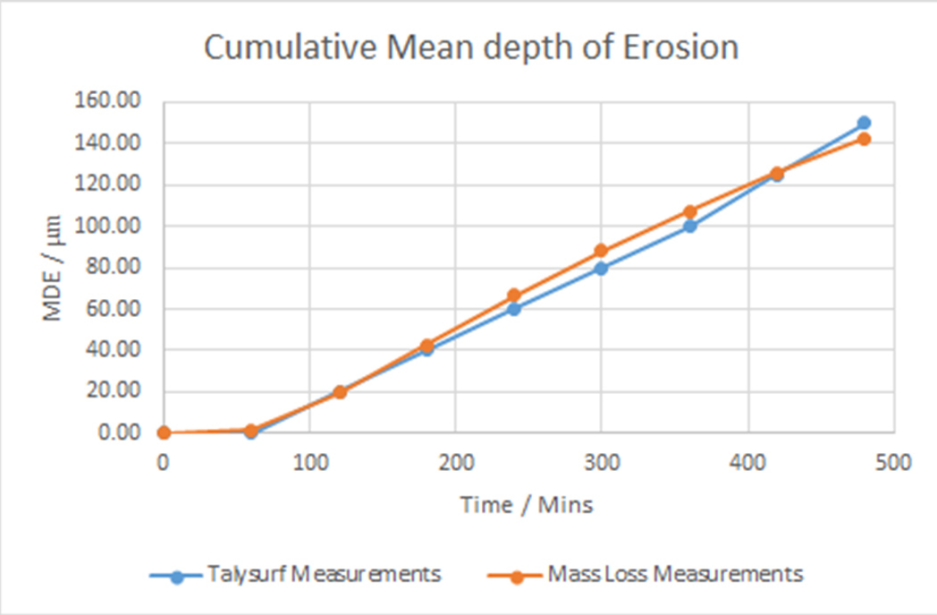

FIG. 6 GRAPH TO SHOW THE CUMULATIVE DEPTH OF EROSION PER HOUR FOR NICKEL 200 AS APPROXIMATED FROM TALYSURF AND MASS LOSS MEASUREMENTS.

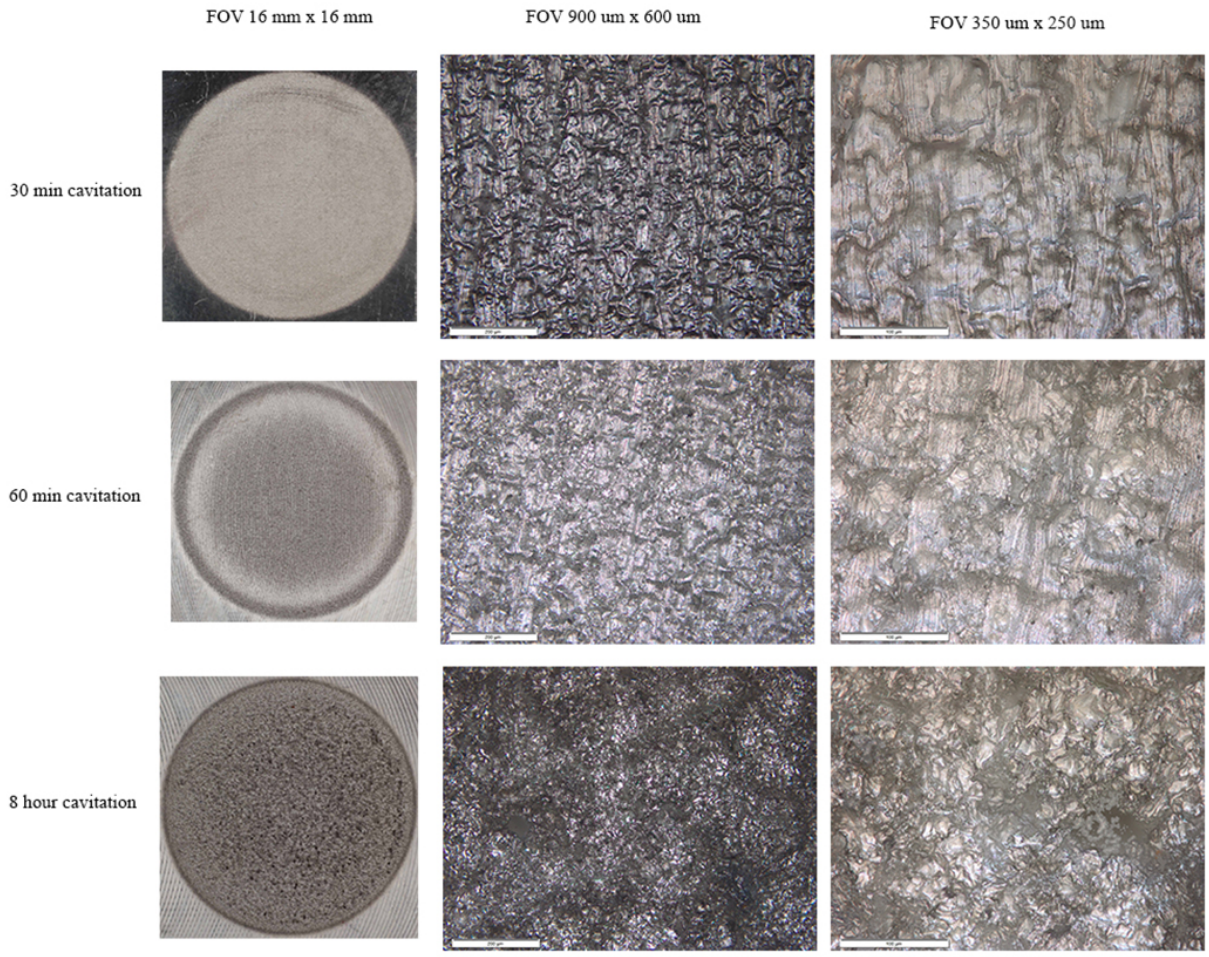

FIG. 7 OPTICAL IMAGES OF THE FORMATION OF CAVITIES OF NICKEL 200 AT 30 MINS, 60 MINS AND 8 HOURS OF CAVITATION TESTING.

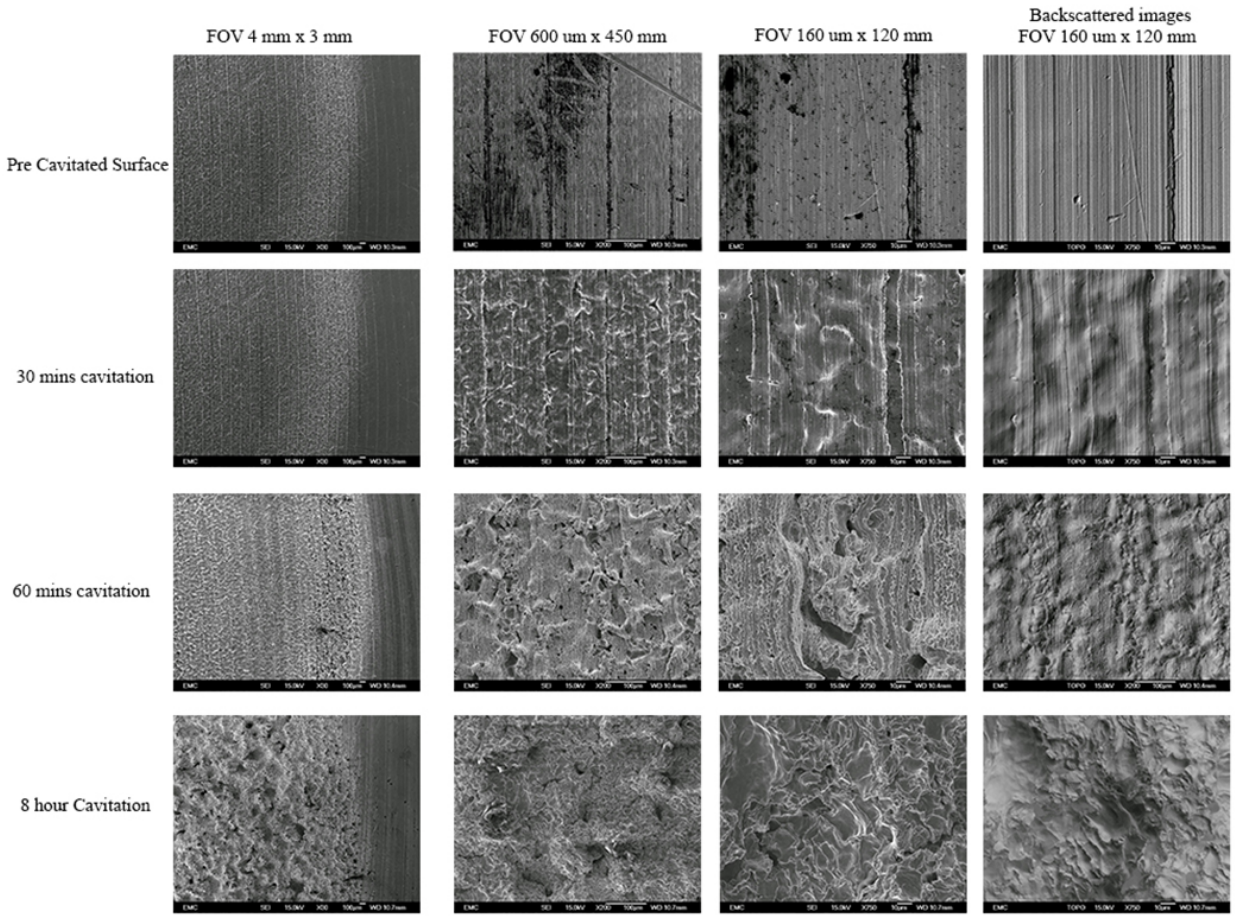

FIG. 8 SEM IMAGES OF THE FORMATION OF CAVITIES OF NICKEL 200 AT 30 MINS, 60 MINS AND 8 HOURS OF CAVITATION TESTING. IMAGES TAKEN FROM THE CENTRE OF THE CAVITATION DAMAGE.

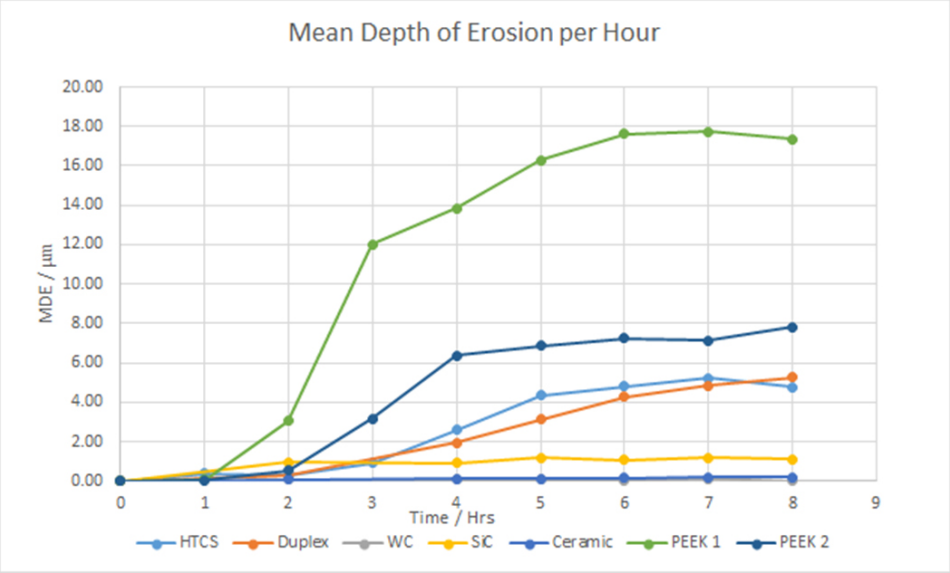

FIG 9. GRAPH TO SHOW THE MEAN DEPTH OF EROSION PER HOUR FOR MATERIALS UNDER TEST.

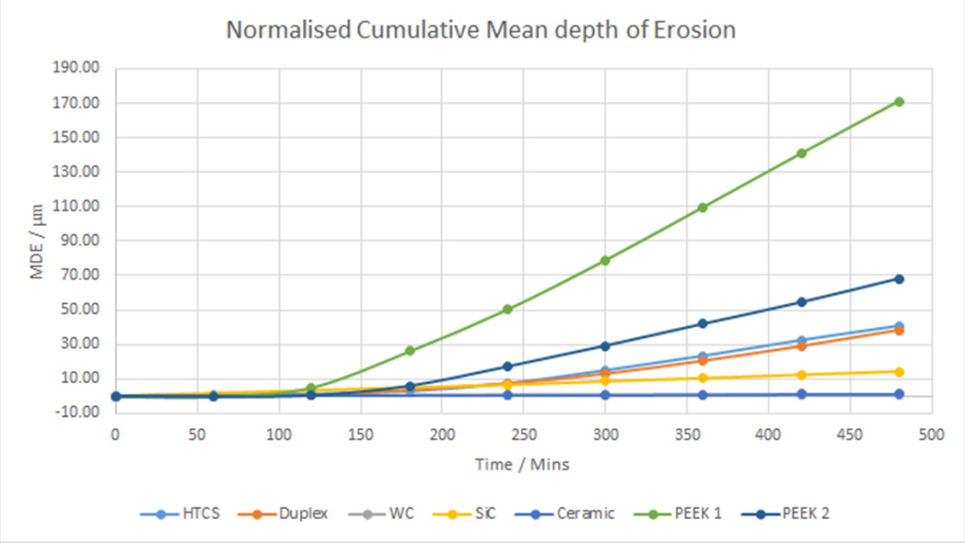

FIG. 10 GRAPH TO SHOW THE NORMALISED CUMULATIVE MEAN DEPTH OF EROSION (DATA FOR WC FOLLOWS THE ZrO_2 LINE).

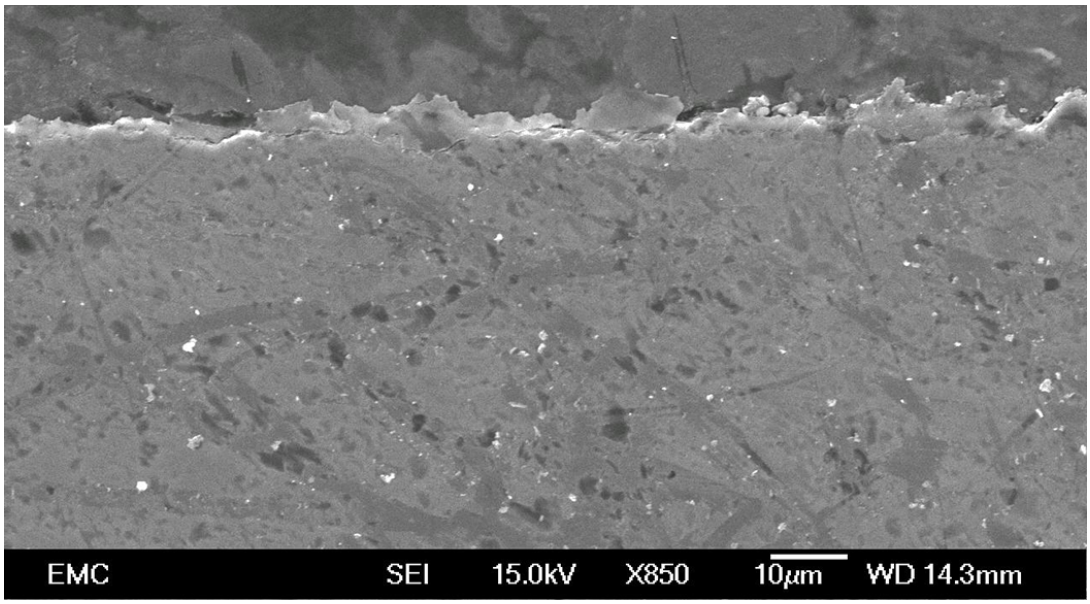

FIG. 11 SEM CROSS SECTION IMAGE AT X850 MAGNIFICATION OF THE ERODED SURFACE OF SILICON CARBIDE.

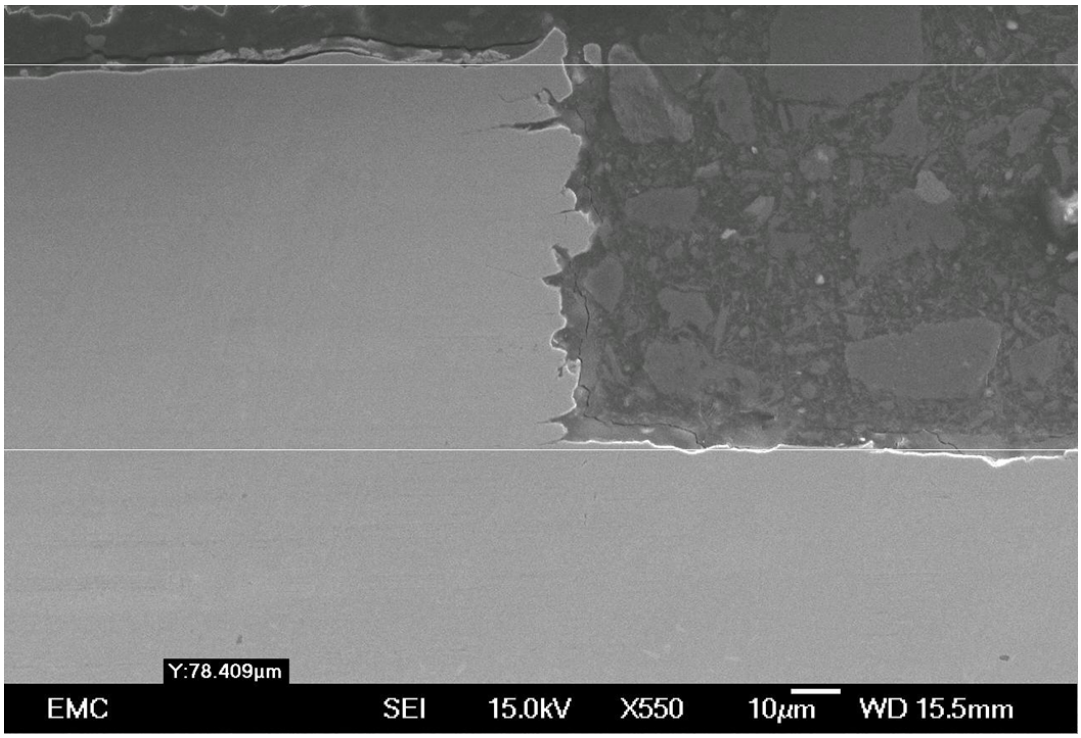

FIG. 12 SEM CROSS SECTION IMAGES AT X550 OF THE STEPPED EDGE OF THE ERODED SURFACE OF DSS. NOTE THE HEIGHT WAS MEASURED (SEE WHITE LINES ON IMAGE) TO BE 78 MM.

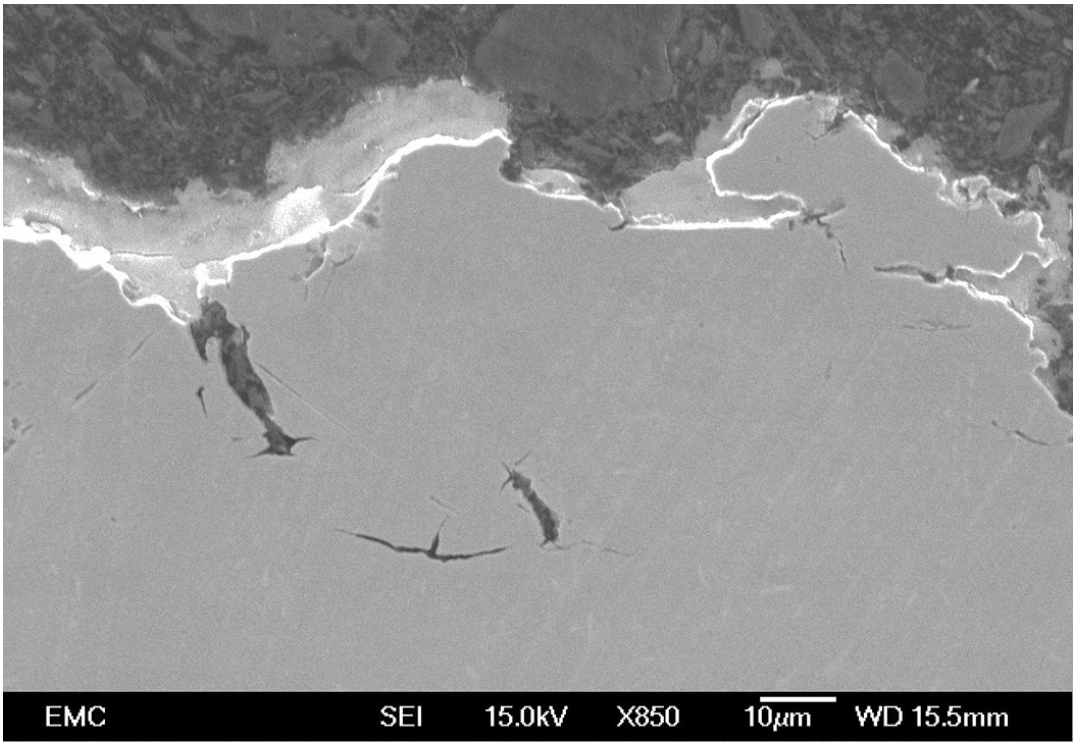

FIG. 13 SEM CROSS SECTION IMAGES AT X850 OF THE ERODED SURFACE OF DSS.

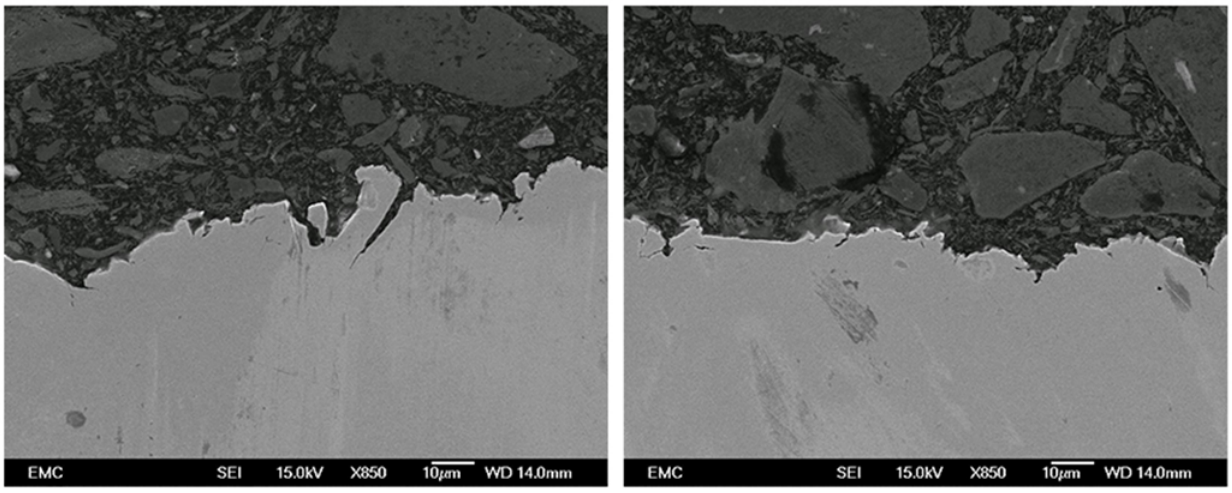

FIG. 14 SEM CROSS-SECTION IMAGES AT X850 MAGNIFICATION OF THE ERODED SURFACE OF HTCS.